A. SUPPLEMENTARY MATERIAL — PART A

FIGURES, TABLES and COMMENTS on:

- the model exploited in the calculations on the dissociation dynamics of the ion, properties of the potentials involved.
- the algorithms used in the Siegert-quantization calculations of the rovibronic resonance energies, total and partial widths
- all rotation-vibration levels supported by the included volcano-like potentials whose dissociation widths are smaller than 10.6 cm^{-1} (lifetimes larger than 0.5 ps).
- variation of the widths with the rotational quantum number in every of 93 different vibronic states the levels belong to.
- densities of rovibronic levels (DOL) and states (DOS); resolutions into contributions of different vibronic levels/states.
- kinetic energy release (KER) spectra from breakup of the ion in the idealized samples with equal population of all levels/states characterized by lifetimes in the range from 1 ps to 5 ns and in the range [0.5 ps, ∞); details on importance of particular vibronic states, on the role of decay into excited fragmentation channels for explaining the experimental spectra[1,2].

Describing dissociation of the ion from its $s_\Omega\, vJMp$ states /$s_\Omega\, vJp$ levels/ for $s{=}X\,^3\Pi$, $a\,^1\Sigma^+$, $b\,^1\Pi$, $A\,^3\Sigma^+$, $c\,^1\Delta$, $d\,^1\Sigma^+$

Fig. A1. Hamiltonian matrices $\mathbf{H}^{Jp} = \left\{ H^{Jp}_{s_\Omega, \widetilde{s}_{\Omega'}} \right\}$

$$\mathbf{H}^{Jp}(r) = -\tfrac{1}{2\mu}\mathbf{I}\tfrac{d^2}{dr^2} + \mathbf{V}^{Jp}(r)$$

$$\begin{aligned} V^{Jp}_{s_\Omega, \widetilde{s}_{\Omega'}}(r) \;=\; & \delta_{s,\widetilde{s}}\,\delta_{\Omega,\Omega'}\left[\tfrac{1}{2\mu r^2}\,E^J(s_\Omega) + V_s(r) + A_\Lambda(r)\,\Lambda(\Omega{-}\Lambda)\right] \\ -\; & \delta_{s,\widetilde{s}}\,\delta_{\Omega',\Omega\pm1}\,\tfrac{1}{2\mu r^2}\,C^{Jp}_{\Omega,\Omega\pm1}(s) + \delta_{\Omega,\Omega'}\,(1-\delta_{s,\widetilde{s}})\,V_{s,\widetilde{s}}(r) \end{aligned}$$

$$\begin{aligned} E^J(s_\Omega) \;&:=\; J(J{+}1){+}S(S{+}1){-}\Omega^2{-}\Sigma^2\,, \qquad \Sigma{=}\Omega{-}\Lambda\,, \\ C^{Jp}_{\Omega,\Omega\pm1}(s) \;&:=\; [J(J{+}1){-}\Omega(\Omega{\pm}1)]^{1/2}\times \\ &\quad\; [S(S{+}1){-}(\Sigma{\pm}1)\Sigma]^{1/2}{\times}N^p(s_\Omega)\,N^p(s_{\Omega\pm1})\,. \end{aligned}$$

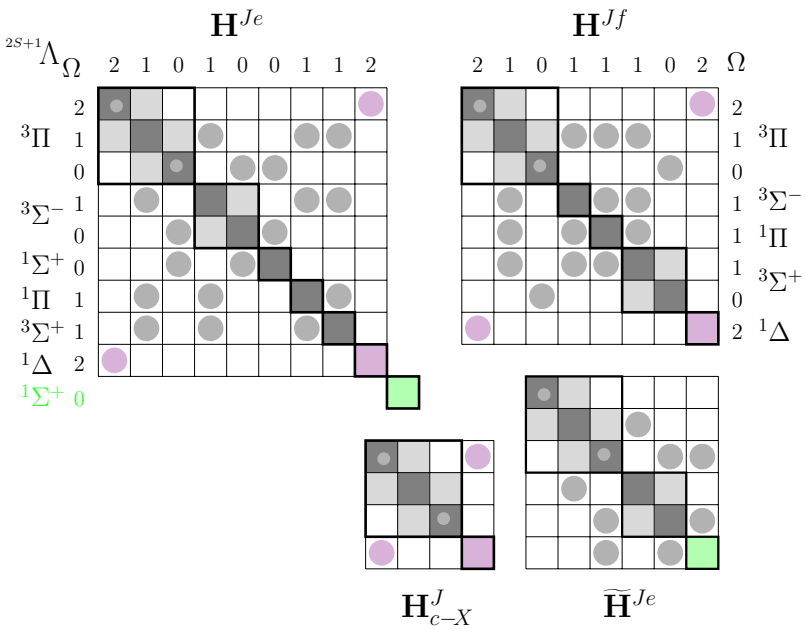

In these schemes,

- the dark gray, violet and green squares represent all the diagonal terms of the matrices except for the SO terms ($\pm A\,^3\Pi$) which are shown explicitly by the small gray circles,
- the large circles — the SO couplings,
- the light gray squares — the **S** uncoupling terms, the factor $N^p(s_\Omega)\,N^p(s_{\Omega\pm1}){=}1$ in the $^3\Pi$ blocks and $\sqrt{2}$ — in the $^3\Sigma$ blocks.

The different colors serve to notify about the fact that the states were not treated on equal footing. Levels in the states X, a, b, and A were generated using the blocks $\mathbf{H}^{Je}_{8\times8}$ and $\mathbf{H}^{Jf}_{7\times7}$ with the gray terms. Since the potential $V_c(r)$ is the least complete of the potentials available from Ref. 3, the matrices with the violet terms were used only in the part of calculation aimed at an estimation of the c-state contribution to the simulated KER spectra. Calculations on levels in the state d had a similar subsidiary purpose. Since none of the SO couplings available from Ref. 4 involves this state, the single Hamiltonian term represented by the green square could only be formed. In other words, only tunneling could be reliably accounted for in the description of dissociation of the ion from its d state levels. A crude estimation of predissociation from these levels was the goal of calculations with the matrix $\ddot{\mathbf{H}}^{Je}$. In this matrix, the SO couplings of the state a are used in the role of the couplings $d\,^1\Sigma^+{-}^3\Sigma^-$ and $d\,^1\Sigma^+{-}^3\Pi$.

Fig. A1b. Effective potentials $V^J_{s_\Omega}(r)$ /:=$V^{Jp}_{s_\Omega,s_\Omega}(r)$/ *

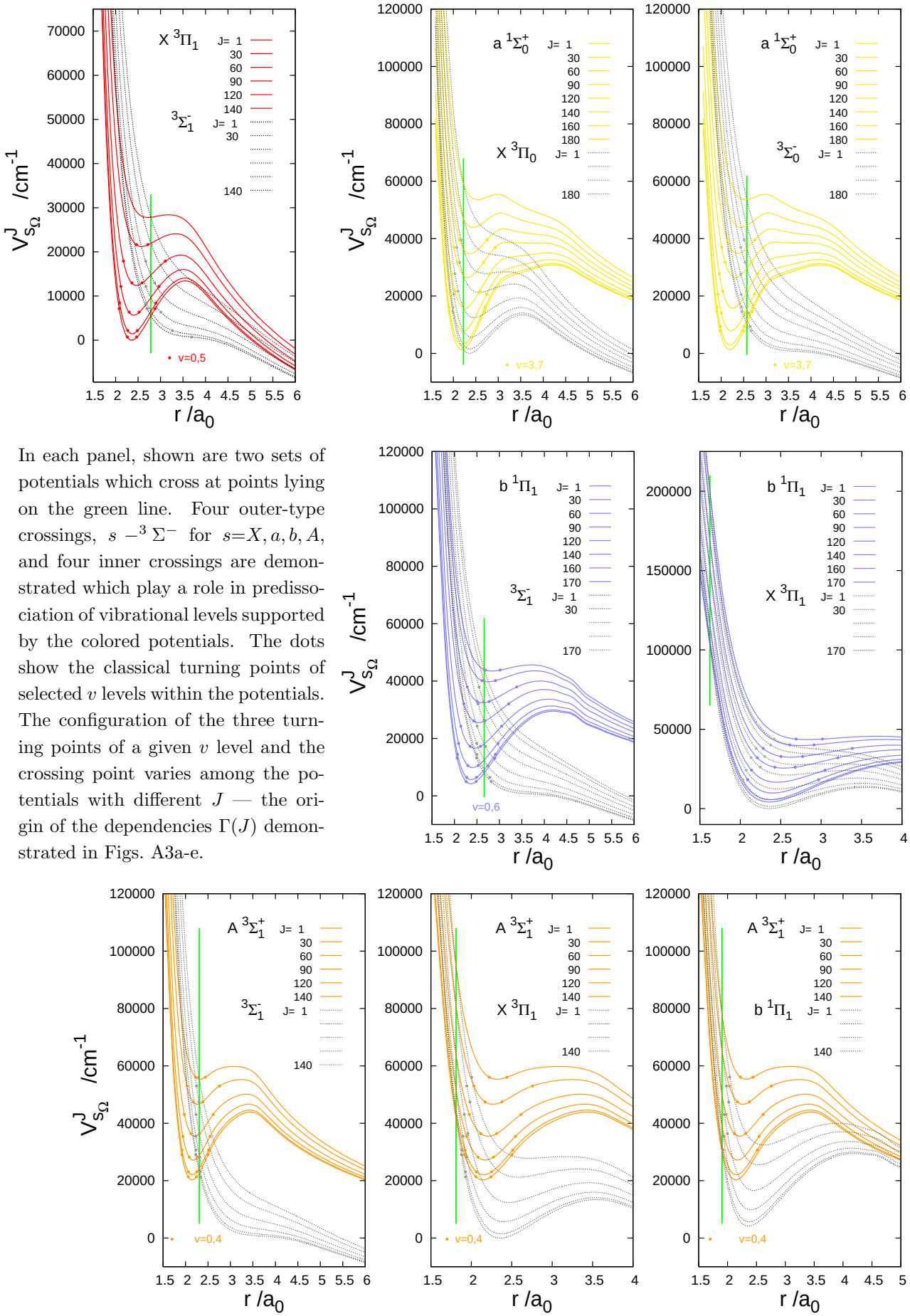

In each panel, shown are two sets of potentials which cross at points lying on the green line. Four outer-type crossings, $s\ -^3\Sigma^-$ for $s{=}X, a, b, A$, and four inner crossings are demonstrated which play a role in predissociation of vibrational levels supported by the colored potentials. The dots show the classical turning points of selected v levels within the potentials. The configuration of the three turning points of a given v level and the crossing point varies among the potentials with different J — the origin of the dependencies $\Gamma(J)$ demonstrated in Figs. A3a-e.

* The potentials of states $c\,^1\Delta$ and $d\,^1\Sigma^+$ are presented in Fig. A4.

Solving equation

$$[\mathcal{E}\mathbf{I} - \mathbf{H}^{Jp}(r)]\,\mathbf{\Psi}^{Jp}(r;\mathcal{E}) = 0 \qquad \mathcal{E}\in C \tag{A1}$$

for RESONANCE ENERGIES, TOTAL AND PARTIAL WIDTHS with THE GENERALIZED LOG-DERIVATIVE METHOD

The basic quantity is the log-derivative matrix $\underset{N\times N}{\mathbf{L}}^{Jp}(r;\mathcal{E})$ of solutions of Eq. (A1), $\frac{d}{dr}\mathbf{\Psi}^{Jp}(r;\mathcal{E}) = \mathbf{L}^{Jp}(r;\mathcal{E})\,\mathbf{\Psi}^{Jp}(r;\mathcal{E})$, which satisfies the Riccati equation

$$\frac{d}{dr}\mathbf{L}^{Jp} + (\mathbf{L}^{Jp})^2 + \mathbf{W}^{Jp} = \mathbf{0} \qquad \text{with} \quad \mathbf{W}^{Jp}(r;\mathcal{E}) = 2\mu[\mathcal{E}\mathbf{I}-\mathbf{V}^{Jp}(r)]\,. \tag{A2}$$

The resonance eigenvalue $\mathcal{E}_n^{Jp}{=}E_n^{Jp}{-}\frac{\imath}{2}\Gamma_n^{Jp}$ is obtained as root of the equation

$$\det\big[\mathbf{L}^{Jp}(r_{\rm m};\mathcal{E}) - \mathbf{L}_{O^+}^{Jp}(r_{\rm m};\mathcal{E})\big] = 0\,, \tag{A3}$$

where $\mathbf{L}^{Jp}(r;\mathcal{E})$ denotes solution of Eq. (A2) satisfying the initial condition $\big[\mathbf{L}^{Jp}(0;\mathcal{E})\big]^{-1}{=}0\mathbf{I}$, and $\mathbf{L}_{O^+}^{Jp}(r;\mathcal{E})$ is a solution started at the point $r{=}r_\infty$ from the matrix $\mathbf{L}_{O^+}^{Jp}(r_\infty;\mathcal{E})$ listed in Eq. (5) of the paper. The matching point $r_{\rm m}$ of the two solutions is chosen near the minimum of the well in the effective potential $V_{s_\Omega}^J(r)$ which supports a vibrational state (v) of energy close to E_n^{Jp} /hence, $n := (s_\Omega, v)$/.

Evaluation of the partial widths requires the resonance function $\mathbf{\Psi}^{nJp}(r){:=}\mathbf{\Psi}^{Jp}(r;\mathcal{E}_n^{Jp})$ at the point r_∞. At the point $r{=}r_{\rm m}$, the function is obtained as vector in the kernel of the matrix $\big[\mathbf{L}^{Jp}(r_{\rm m};\mathcal{E}_n^{Jp}) - \mathbf{L}_{O^+}^{Jp}(r_{\rm m};\mathcal{E}_n^{Jp})\big]$. The value at r_∞ is determined with the help of the L propagator[5] of solutions of Eq. (A1) over the interval $[r_{\rm m}, r_\infty]$

$$\begin{pmatrix} \frac{d}{dr}\mathbf{\Psi}^{Jp}(r_{\rm m}) \\ \frac{d}{dr}\mathbf{\Psi}^{Jp}(r_\infty) \end{pmatrix} = \mathcal{L}^{Jp}(r_{\rm m}, r_\infty)\begin{pmatrix} \mathbf{\Psi}^{Jp}(r_{\rm m}) \\ \mathbf{\Psi}^{Jp}(r_\infty) \end{pmatrix}, \quad \mathcal{L}^{Jp} = \begin{pmatrix} \mathcal{L}_1^{Jp} & \mathcal{L}_2^{Jp} \\ \mathcal{L}_3^{Jp} & \mathcal{L}_4^{Jp} \end{pmatrix}, \quad \text{(dependence on } \mathcal{E} \text{ omitted).}$$

Namely,

$$\mathbf{\Psi}^{nJp}(r_\infty) = \big[\mathbf{L}_{O^+}^{Jp}(r_\infty) - \mathcal{L}_4^{Jp}(r_{\rm m}, r_\infty)\big]^{-1}\mathcal{L}_3^{Jp}(r_{\rm m}, r_\infty)\,\mathbf{\Psi}^{nJp}(r_{\rm m})\,. \tag{A4}$$

The block $\mathcal{L}_4^{Jp}(r_{\rm m}, \bar{r})$ of the L propagator, considered as function of the upper boundary $\bar{r}$ of the propagation interval, satisfies Riccati equation identical to Eq. (A2) and the initial condition, for zero-length interval, is[5]: $\lim_{\epsilon\to O^+}\mathbf{L}^{Jp}(r_{\rm m}, r_{\rm m}{+}\epsilon){=}1/\epsilon\mathbf{I}$. So, the log-derivative matrix $\mathbf{L}^{Jp}(r_{\rm m})$ used in Eq. (A3) is practically the same as $\mathcal{L}_4^{Jp}(0, r_{\rm m})$. The respective differential equations for the other blocks of the propagator are linear; details can be found in Ref. 5.

Knowing the vector $\mathbf{\Psi}^{nJp}(r_\infty)$ is sufficient for the evaluation of the probabilities $p_{n,c}^{Jp}$ of decay of nJp resonance into open channels c, with $\varepsilon_c{<}E_n^{Jp}$, according to formula (7) of the paper. Obtaining the partial widths is only a matter of multiplication by the total width Γ_n^{Jp} which is already available as $-2\,\mathrm{Im}\,\mathcal{E}_n^{Jp}$.

However, in order to check numerical accuracy of the determined Siegert-eigenvalues, the total widths of a number of resonances were also evaluated according to the following 'flux formula'[6]

$$\Gamma_n^{Jp} = \frac{\big(\mathbf{\Psi}^{nJp}\,|\mathbf{C}(\bar{r})\,\mathbf{\Psi}^{nJp}\big)}{\big(\mathbf{\Psi}^{nJp}\,|I_{[0,\bar{r}]}\,\mathbf{\Psi}^{nJp}\big)}\,, \tag{A5}$$

where $I_{[0,\bar{r}]}(r)$ denotes the projector on the $[0,\bar{r}]$ interval of r coordinate, valid for any $\bar{r}{>}0$.

The formula was evaluated for $\bar{r}{=}r_{\rm m}$ and $\bar{r}{=}r_\infty$. So, the values of the matrix element in the nominator could be obtained using the quantities already evaluated: $\mathbf{\Psi}^{nJp}(r_{\rm m})$, $\mathbf{L}^{Jp}_{O^+}(r_{\rm m};\mathcal{E}^{Jp}_n)$, and $\mathbf{L}^{Jp}_{O^+}(r_\infty;\mathcal{E}^{Jp}_n)$ — in the eigenvalue search, and $\mathbf{\Psi}^{nJp}(r_\infty)$ — in the decay probability calculations. Extra calculations were needed to evaluate the matrix element in the denominator. These calculations were done with the help of the generalized log-derivative algorithms for free-free transition amplitudes[7,8]. Directly evaluated by the algorithms are the integrals

$$\underset{N\times N}{\mathbf{J}^{\alpha,\beta}_{[r',r'']}} = \int_{r'}^{r''} \mathbf{\Psi}^{\alpha\,\dagger}_{[r',r'']}(r)\,\mathbf{\Psi}^{\beta}_{[r',r'']}(r)\,dr$$

between ($N{\times}N$ matrices of) functions $\mathbf{\Psi}^{\alpha}_{r',r''}(r)$ and $\mathbf{\Psi}^{\beta}_{r',r''}(r)$, with $\alpha,\beta{=}+,-$, which are solutions of the following boundary-value problems for Eq. (A1) with $\mathcal{E}{=}\mathcal{E}^{Jp}_n$ / for clarity, the resonance labels are omitted here/

$$[\mathbf{I}\frac{d^2}{dr^2}+\mathbf{W}(r;\mathcal{E})]\,\mathbf{\Psi}^{\pm}_{[r',r'']}(r)=\mathbf{0}\,, \tag{A6}$$

$$\mathbf{\Psi}^{\pm}_{[r',r'']}(r')=\begin{cases}\mathbf{I}\\ \mathbf{0}\end{cases},\quad \mathbf{\Psi}^{\pm}_{[r',r'']}(r'')=\begin{cases}\mathbf{0}\\ \mathbf{I}\end{cases}. \tag{A7}$$

The probabilities $\left(\mathbf{\Psi}^{nJp}\,|I_{[0,\bar{r}]}\,\mathbf{\Psi}^{nJp}\right)$ for $\bar{r}=r_{\rm m},r_\infty$ can be expressed in terms of the $\mathbf{J}$ integrals as follows

$$\left(\mathbf{\Psi}^{nJp}\,|I_{[0,\,r_{\rm m}]}\,\mathbf{\Psi}^{nJp}\right) = \mathbf{\Psi}^{nJp\,\dagger}(r_{\rm m})\,\mathbf{J}^{-,-}_{[0,r_{\rm m}]}\,\mathbf{\Psi}^{nJp}(r_{\rm m})\,, \tag{A8}$$

$$\begin{aligned}\left(\mathbf{\Psi}^{nJp}\,|I_{[0,r_\infty]}\,\mathbf{\Psi}^{nJp}\right) &= \left(\mathbf{\Psi}^{nJp}\,|I_{[0,r_{\rm m}]}\,\mathbf{\Psi}^{nJp}\right)\\ &+ \mathbf{\Psi}^{nJp\,\dagger}(r_{\rm m})\,\mathbf{J}^{-,-}_{[r_\infty,r_{\rm m}]}\,\mathbf{\Psi}^{nJp}(r_{\rm m})\\ &+ \mathbf{\Psi}^{nJp\,\dagger}(r_\infty)\,\mathbf{J}^{-,-}_{[r_{\rm m},r_\infty]}\,\mathbf{\Psi}^{nJp}(r_\infty)\\ &+ \left[\mathbf{\Psi}^{nJp\,\dagger}(r_\infty)\,\mathbf{J}^{-,+}_{[r_{\rm m},r_\infty]}\,\mathbf{\Psi}^{nJp}(r_{\rm m})\;+\;h.c\right].\end{aligned} \tag{A9}$$

In the expression for $\left(\mathbf{\Psi}^{nJp}\,|I_{[r_{\rm m},\,r_\infty]}\,\mathbf{\Psi}^{nJp}\right)$ /the three latter lines/, the integral $\mathbf{J}^{-,-}_{[r_\infty,r_{\rm m}]}$ is inserted in place of the equivalent $\mathbf{J}^{+,+}_{[r_{\rm m},r_\infty]}$ since it is more convenient to compute.

Below collected are the formulas of the original[9] and the generalized log-derivative algorithms[5,7,8] which were used to evaluate the matrices $\mathcal{L}_4(r',r'')$, $\mathcal{L}_3(r',r'')$, $\mathbf{J}^{-,-}_{[r',r'']}$, and $\mathbf{J}^{-,+}_{[r',r'']}$. The formulas concerning the latter integral have not been explicitly listed before.

$$\mathbf{z}_0^{-1}=0\mathbf{I}\,,\quad \mathbf{u}_0=\tfrac{h^2}{3}\mathbf{I}\,,\quad \mathbf{p}_1=-\tfrac{1}{h}\mathbf{I}\,,\quad \mathbf{t}_1=0\mathbf{I}\,,$$

$$\mathbf{p}_l=\mathbf{z}_{l-1}^{-1}\,\mathbf{p}_{l-1}\,,$$

$$\mathbf{t}_l=\mathbf{z}_{l-1}^{-1\,\dagger}\,(\mathbf{t}_{l-1}-\mathbf{u}_{l-1}\,\mathbf{p}_l)\,,$$

$$\mathbf{u}_l=\mathbf{z}_{l-1}^{-1\,\dagger}\,\mathbf{u}_{l-1}\,\mathbf{z}_{l-1}^{-1}+\begin{cases}\frac{h^2}{48}\mathbf{g}_l^\dagger\,\mathbf{g}_l & \text{for } l \text{ odd},\\ \frac{2h^2}{3}\mathbf{I} & \text{for } l \text{ even},\end{cases}$$

$$\mathbf{z}_l=-\mathbf{z}_{l-1}^{-1}+\begin{cases}-6\mathbf{I}+\mathbf{g}_l & \text{for } l \text{ odd},\\ 2\mathbf{I}-\frac{2h^2}{3}\mathbf{w}_l & \text{for } l \text{ even},\end{cases}$$

$$l{=}1,2,\ldots,2M,$$

$$\mathbf{J}^{-,-}_{[r',r'']} = (\mathbf{u}_{2M} - \tfrac{h^2}{3}\mathbf{I})/h\,,$$

$$\mathbf{J}^{-,+}_{[r',r'']} = \mathbf{t}_{2M}\,,$$

$$\mathcal{L}_3(r',r'') = \mathbf{p}_{2M}\,,$$

$$\mathcal{L}_3(r',r'') = (\mathbf{z}_{2M} - \mathbf{I} + \tfrac{h^2}{3}\mathbf{w}_{2M})/h\,,$$

where $$\mathbf{g}_l = [\tfrac{1}{8}\mathbf{I}+\tfrac{h^2}{48}\mathbf{w}_l]^{-1}\,, \quad \mathbf{w}_l=\mathbf{W}(r_l)\,,$$

$$r_l=r_0+lh\,, \quad r_0 = r'\,, \quad r_{2M}=r''\,.$$

An illustration of performance of the algorithms is provided in Table AI on a selection of levels whose widths Γ vary in a wide range, from 6×10^{-17} to 10 cm^{-1}. Relative deviations between the values $\Gamma(\bar{r}=r_{\rm m})$, $\Gamma(r_\infty)$ (resulting from Eq. (A5)) and Γ (from Siegert eigenvalue) are shown in the columns marked with ••. The deviations are generally of the size of 10^{-8}–10^{-9}.

Two other practical aspects are illustrated in Table AI:

(i) adequacy of the asymptotic boundary condition in the WKB form, Eq. (3) of the paper. It can be assessed by looking at stability of results against shifts of the position r_∞ of the boundary. Standard deviations $\sigma(X)$ relative to mean values $\overline{X}$ in the sets of results calculated with 5 positions r_∞, between 13.5 and 18.5 a_0, for each of the three characteristics X of the levels, E, Γ, and p_1, are shown in the three columns marked with •. The values of $\sigma(\Gamma)/\overline{\Gamma}$ are substantially larger than the deviations in the •• columns. In worst cases, only five significant digits of Γ appear stable. The values of $\sigma(p_1)/\overline{p_1}$ indicate that the probabilities p_1, if much smaller than 0.001% may be uncertain even on second significant figure. Obviously, these tiny probabilities are totally unimportant for the main purpose of the present calculations — the determination of the global characteristics KERS, KERL. The accuracy of the widths is sufficient and the accuracy of the energies, as indicated by $\sigma(E)/\overline{E}$, is by far better than sufficient for this purpose.

(ii) possibility of determining the partial widths, especially the most important ones that concern the $A\,^3\Sigma^+$-state levels, in a way not requiring evaluation of the resonance functions. The way is suggested by the observation made in the previous study[10] that the total widths of the vibronic $A\,v$ levels may reasonably be approximated by sums of widths due to the three individual curve-crossings involved, each evaluated separately from the others. The entries in the last column illustrate how accurate probabilities p_1 can be obtained from such an approach. Relative deviations from the 'exact' values do not exceed a few per cent provided these values (in column 6) are not too small, i.e. not smaller than ∼1%.

TABLE AI: A demonstration of numerical accuracy of characteristics of ro-vibronic levels of the CO^{++} ion determined in calculations using the Hamiltonian matrices $\mathbf{H}^{Je}_{8\times 8}$ and $\mathbf{H}^{Jf}_{7\times 7}$.
• Stability of energies (E), total widths (Γ), and probabilities of decay into first excited fragmentation channel (p_1) with respect to the position r_∞ of the asymptotic boundary condition /Eq. (3) of the paper/. •• Consistency of Γ values obtained from the Siegert-eigenvalues and from the 'flux formula', Eq. (A5).
Behind the vertical line — an illustration of accuracy achievable in determining the probabilities p_1 from truncated Hamiltonian matrices not allowing for transitions to the ground dissociation channel.

Level			$\overline{X}$ [a]			• $\sigma(X)/\overline{X}$ [b]			•• rmsd$(X,Y)/\overline{Y}$ [c]		$\lvert\overline{X}/\overline{Y}-1\rvert$
$^{2S+1}\Lambda_\Omega$	v	J^p	$X{=}E$ cm^{-1}	$X{=}\Gamma$ cm^{-1}	$X{=}p_1$ %	$X{=}E$	$X{=}\Gamma$	$X{=}p_1$	$X{=}\Gamma(r_\mathrm{m})$ $Y{=}\Gamma$	$X{=}\Gamma(r_\mathrm{m})$ [d] $Y{=}\Gamma(r_\infty)$	$X{=}\widetilde{p}_1$ [e] $Y{=}p_1$
$^3\Pi_2$	0	2^e	655.49	5.85 (−17)[f]	2.2 (−11)	1 (−11)	3 (−7)	2 (−1)	3 (−09)	2 (−08)	
	0	143^e	28712.18	7.51 (+01)	1.4 (−06)	9 (−09)	4 (−5)	2 (−3)	2 (−09)	5 (−09)	
$^3\Pi_1$	0	1^e	718.95	4.95 (−14)	2.9 (−12)	9 (−12)	3 (−7)	7 (−5)	3 (−09)	3 (−09)	
	0	140^e	28081.49	1.63 (−00)	1.4 (−06)	2 (−10)	7 (−6)	8 (−5)	6 (−09)	1 (−08)	
$^3\Pi_0$	0	0^e	780.77	1.46 (−13)	2.1 (−22)	9 (−12)	8 (−8)	1 (−4)	7 (−10)	7 (−10)	
	11	23^e	13566.58	1.00 (+01)	3.1 (−06)	3 (−09)	1 (−5)	5 (−3)	5 (−09)	6 (−09)	
$^1\Sigma^+$	1	70^e	12864.55	7.37 (−03)	1.3 (−06)	8 (−12)	2 (−5)	3 (−4)	7 (−09)	6 (−09)	
	1	71^e	13115.03	6.50 (−05)	1.5 (−06)	6 (−12)	3 (−5)	2 (−4)	2 (−09)	6 (−09)	
	2	15^e	6374.64	2.41 (−01)	2.3 (−09)	1 (−10)	8 (−6)	3 (−2)	1 (−08)	7 (−09)	
	2	165^e	49141.74	1.77 (−01)	16.7	3 (−11)	1 (−5)	2 (−5)	1 (−09)	1 (−08)	1 (−3)
	7	130^e	40353.32	7.23 (−01)	78.9	2 (−11)	4 (−6)	1 (−5)	3 (−09)	2 (−09)	4 (−3)
	10	110^e	36795.95	2.98 (−02)	32.4	7 (−12)	3 (−5)	3 (−5)	1 (−08)	1 (−08)	7 (−3)
	21	5^e	29893.02	4.37 (−02)	2.3	5 (−13)	1 (−7)	6 (−6)	2 (−08)	2 (−08)	1 (−3)
$^1\Pi_1$	0	180^e	47439.04	2.50 (−02)	73.1	3 (−12)	8 (−6)	8 (−6)	2 (−08)	1 (−08)	6 (−3)
	6	154^e	42085.45	1.35 (−00)	96.3	2 (−11)	1 (−6)	5 (−6)	2 (−08)	2 (−08)	4 (−3)
	8	139^e	38954.37	5.58 (−02)	5.0	3 (−11)	3 (−5)	3 (−5)	7 (−09)	6 (−09)	4 (−3)
	20	40^e	29051.40	6.54 (−03)	5.5 (−01)	4 (−12)	5 (−6)	4 (−6)	2 (−08)	9 (−07)	4 (−3)
	22	25^e	29356.56	6.06 (−01)	96.5	1 (−12)	5 (−8)	4 (−6)	9 (−09)	9 (−09)	4 (−3)
$^3\Sigma^+_0$	0	0^f	21324.28	2.02 (−04)	2.2 (−06)	5 (−13)	1 (−7)	3 (−7)	2 (−07)	1 (−07)	
	0	95^f	38405.24	1.19 (−03)	11.6	5 (−13)	2 (−7)	2 (−6)	2 (−08)	2 (−08)	1 (−2)
	5	5^f	30831.30	7.01 (−02)	74.4	2 (−12)	4 (−7)	3 (−6)	4 (−09)	3 (−09)	2 (−2)
$^3\Sigma^+_1$	0	60^f	28402.01	3.95 (−04)	5.8 (−07)	4 (−13)	2 (−6)	7 (−7)	4 (−08)	5 (−08)	
	0	78^f	32475.72	6.18 (−04)	6.7	3 (−13)	1 (−6)	2 (−6)	2 (−08)	1 (−08)	1 (−2)
	0	79^f	32758.93	2.75 (−03)	78.8	5 (−13)	2 (−7)	3 (−7)	3 (−07)	1 (−07)	2 (−2)
	0	80^f	33045.42	9.84 (−04)	38.8	1 (−12)	6 (−7)	1 (−6)	4 (−09)	8 (−09)	2 (−2)
	0	150^e	60668.16	2.06 (−03)	1.9 (−01)	7 (−13)	1 (−5)	1 (−5)	5 (−08)	6 (−08)	2 (−1)
	2	110^e	46705.10	3.88 (−03)	56.3	5 (−13)	2 (−5)	2 (−5)	2 (−08)	9 (−09)	4 (−2)
	4	120^e	52989.81	3.45 (−03)	89.9	3 (−13)	1 (−6)	1 (−6)	4 (−08)	6 (−08)	3 (−2)

[a] $\overline{X} = \frac{1}{5}\sum_{i=0}^{4} X_i$ where X_i denotes the value obtained from calculations with the asymptotic boundary condition placed at $r_\infty = 14.5 + i{\times}1.0\,a_0$.

[b] $\sigma(X) = \left[\frac{1}{5}\sum_{i=0}^{4}(X_i - \overline{X})^2\right]^{1/2}$. [c] rmsd$(X,Y) = [\frac{1}{5}\sum_{i=0}^{4}(X_i - Y_i)^2]^{1/2}$.

[d] $\Gamma(\bar{r})$ for $\bar{r} = r_\mathrm{m}, r_\infty$ obtained from the 'flux formula'.

[e] $\widetilde{p}_1 = \widetilde{\Gamma}_1/\Gamma$ where $\widetilde{\Gamma}_1$ denotes approximate partial width for decay into the first excited channel obtained as total width in calculations with appropriately reduced number of coupled spin-orbit states $^{2S+1}\Lambda_\Omega(:=s_\Omega)$ in the Hamiltonian matrix. Single state s_Ω was retained to obtain $\widetilde{\Gamma}_1$ of rovibrational levels in the singlet states $s{=}a\,^1\Sigma^+$ and $s{=}b\,^1\Pi$. Two spin-orbit states, $b\,^1\Pi$ and $A\,^3\Sigma^+_1$, were retained in calculations on e parity levels in the state $s{=}A$ and three states, $b\,^1\Pi$, $A\,^3\Sigma^+_1$, and $A\,^3\Sigma^+_0$ — in calculations on f parity levels in $s{=}A$.

[f] Numbers in parentheses are powers of 10.

Fig. A2. Energies* of $^{2S+1}\Lambda^{\epsilon}_{\Omega}\, vJp$ levels for $^{2S+1}\Lambda^{\epsilon} = X\,^3\Pi$, $a\,^1\Sigma^+$, $b\,^1\Pi$, and $A\,^3\Sigma^+$

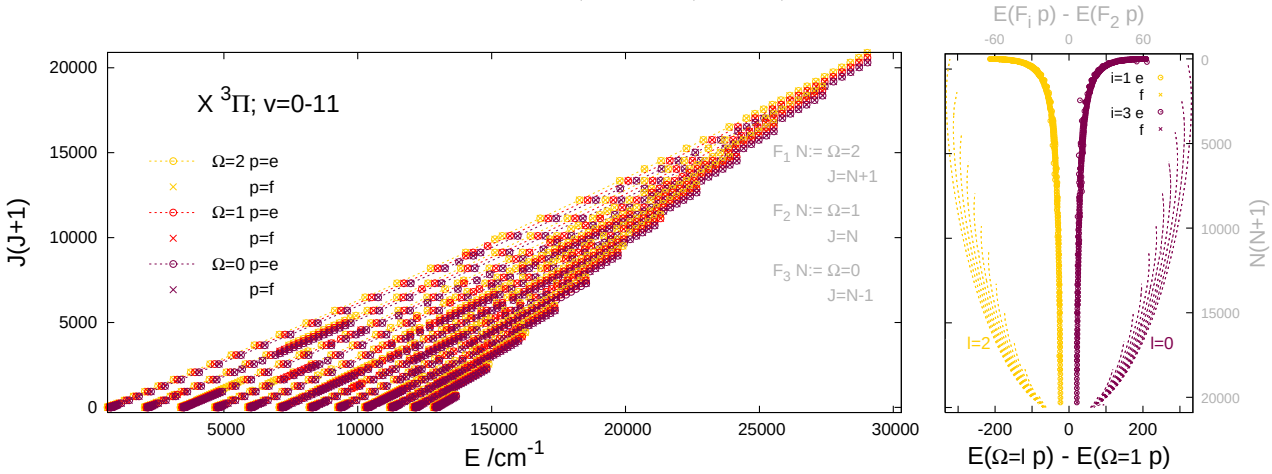

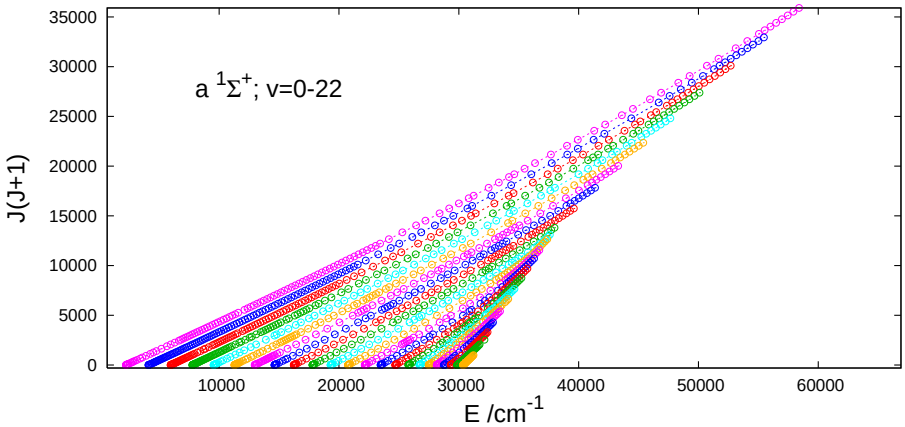

Upper right: The splitting of energies in the $X\,^3\Pi$ state. The splitting $f-e$ of $\Omega\,J$ or F_iN levels is very small, $\lesssim$0.1 cm^{-1}, except for cases of accidental near-degeneracy, mostly with the $a\,^1\Sigma^+$ state levels, see Fig. A3b and Table BI.

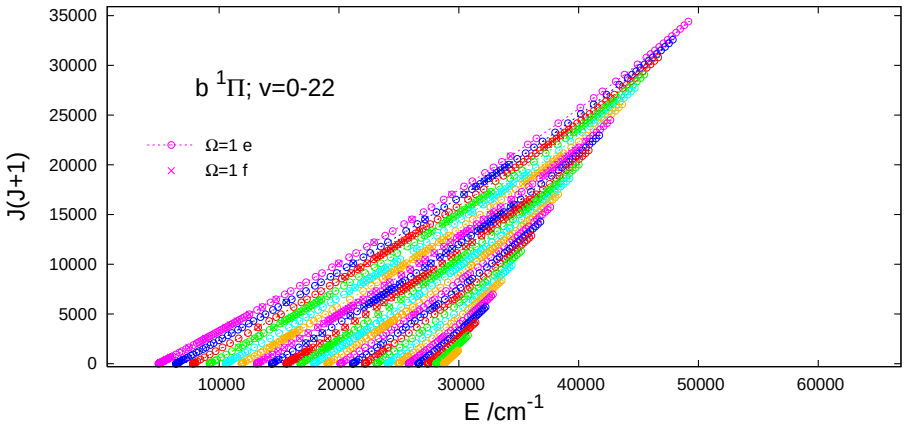

The symbols in all panels of the figure represent the energies actually calculated. The other were obtained by interpolation.

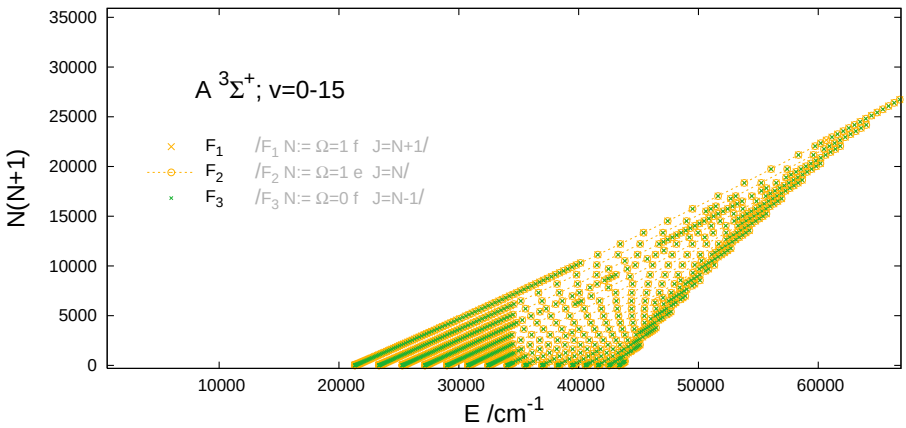

The energies of F_1N, F_2N, and F_3N levels of the $A\,^3\Sigma^+$ state are almost degenerate in the model. See Tables AIII and BIV.

* The energies are relative to the minimum of the X-state potential well.

TABLE AII: Rotational energies of $CO^{2+}(^3\Pi_\Omega\, v)$. Dependence on the number J represented by the polynomial: $E(^3\Pi_\Omega;\, J) = E^0 + B[J(J{+}1) + 1 - 2\Omega(\Omega{-}1)] + C[J(J{+}1) + 1 - 2\Omega(\Omega{-}1)]^2$.

Parameters $E^0(\Omega, v)$, $B(\Omega, v)$, and $C(\Omega, v)$ of fitting to the calculated values $E(^3\Pi_\Omega\, v\, J\, p{=}f)$ [a] in the range J=0−10. Vibrational energies E_{Xv} from the JP04 model of Ref. 10 are enclosed for comparison with the parameters $E^0(\Omega{=}1, v)$ [b]. All entries are in cm^{-1}.

	E_{Xv}	E^0			B			$C \times 10^6$		
v		Ω=0 [c]	Ω=1	Ω=2 [c]	Ω=0	Ω=1	Ω=2	Ω=0	Ω=1	Ω=2
0	714.19	65.12	714.27	−63.27	1.640	1.560	1.495	−46	0	23
1	2101.04[b]	65.13	2102.94[b]	−63.30	1.607	1.531	1.468	−44	−1	21
2	3437.62	65.13	3437.45	−63.29	1.575	1.501	1.440	−42	−2	19
3	4721.41	65.14	4721.16	−63.21	1.540	1.470	1.411	−40	−3	17
4	5953.86[b]	65.02	5951.41[b]	−63.15	1.505	1.437	1.381	−38	−4	15
5	7128.46	64.57	7128.34	−63.30	1.468	1.403	1.350	−37	−4	12
6	8248.75	64.46	8248.65	−62.93	1.429	1.368	1.316	−35	−6	10
7	9310.92	64.06	9310.88	−62.61	1.388	1.330	1.281	−34	−7	8
8	10312.60	63.43	10312.52	−62.20	1.345	1.290	1.243	−34	−8	5
9	11247.84[b]	62.58	11248.50[b]	−61.43	1.297	1.245	1.202	−34	−11	2
10	12110.80	61.20	12110.73	−60.08	1.242	1.193	1.153	−36	−14	−2
11	12879.01	58.43	12879.17	−57.43	1.163	1.120	1.084	−48	−27	−15

[a] f-parity levels are better suited for the fitting because they are free of perturbations by ro-vibrational levels of the state $a\,^1\Sigma^+$. Root-mean-square deviations between the values calculated and the values resulting from the fits: rms dev $\lesssim 1{\times}10^{-3}$ cm^{-1}.

[b] The value of $E_{X\,v}$ deviating more than ± 0.5 cm^{-1} from the value of $E^0(\Omega{=}1)$ testifies on perturbation by a close vibrational level of the state $a\,^1\Sigma^+$. [c] Given relative to the value for the Ω=1 component.

TABLE AIII: Rotational energies of $CO^{2+}(^3\Sigma^+ v)$. Dependence on the number N represented by the polynomial: $E(^3\Sigma^+\, v\, F_i; N) = E^0 + B[N(N+1)] + C[N(N+1)]^2$.

Parameters $E^0(v, F_i)$, $B(v, F_i)$, and $C(v, F_i)$ of fitting to calculated energies in the range N=0−10 [a].

	E^0			B	$C \times 10^6$				E^0			B	$C \times 10^6$		
v	F_1 [b]	F_2 [c]	F_3 [b]	F_2 [d]	F_1 [b]	F_2	F_3 [b]	v	F_1 [b]	F_2 [c]	F_3 [b]	F_2 [d]	F_1 [b]	F_2	F_3 [b]
0	−0.03	21320.56	−0.05	1.898	1	−7	−2	8	−0.02	35538.41	−0.03	1.629	1	−12	−1
1	−0.04	23324.53	−0.06	1.873	2	−7	−2	9	−0.02	36941.33	−0.03	1.579	1	−13	−1
2	−0.04	25275.56	−0.06	1.848	2	−7	−2	10	−0.01	38245.78	−0.02	1.528	1	−13	−1
3	−0.03	27169.47	−0.04	1.820	2	−8	−1	11	−0.01	39455.68	−0.01	1.475	0	−14	0
4	−0.04	28999.49	−0.07	1.789	2	−8	−2	12	0.00	40574.45	−0.01	1.421	1	−16	0
5	−0.03	30757.66	−0.05	1.755	2	−9	−2	13	0.00	41604.00	0.00	1.365	0	−17	0
6	−0.03	32438.58	−0.05	1.717	1	−9	−2	14	0.00	42541.99	0.00	1.302	0	−22	0
7	−0.02	34035.51	−0.04	1.676	1	−10	−1	15	0.00	43368.77	0.00	1.213	0	−37	0

[a] The energy of F_3 N=1 level was excluded from the set for each v. rms dev$<3{\times}10^{-3}$, usually $\ll 10^{-3}$ cm^{-1}.

[b] Relative to the value for the F_2 component.

[c] $E^0(v, F_2)$ agrees with the respective vibrational energy $E_{A\,v}$ from the JP04A model of Ref. 10 with deviation smaller than 0.005 cm^{-1} for v=0−14 and smaller than 0.05 cm^{-1} for v=15.

[d] The values of B for the F_1 and F_3 components are identical to the value for F_2 in all digits shown.

Fig. A3a. $\mathbf{CO}^{2+}(X\,^3\Pi_\Omega)$

Widths (Γ) and lifetimes (τ) of vJp levels

as functions of the number J and level's position (E)

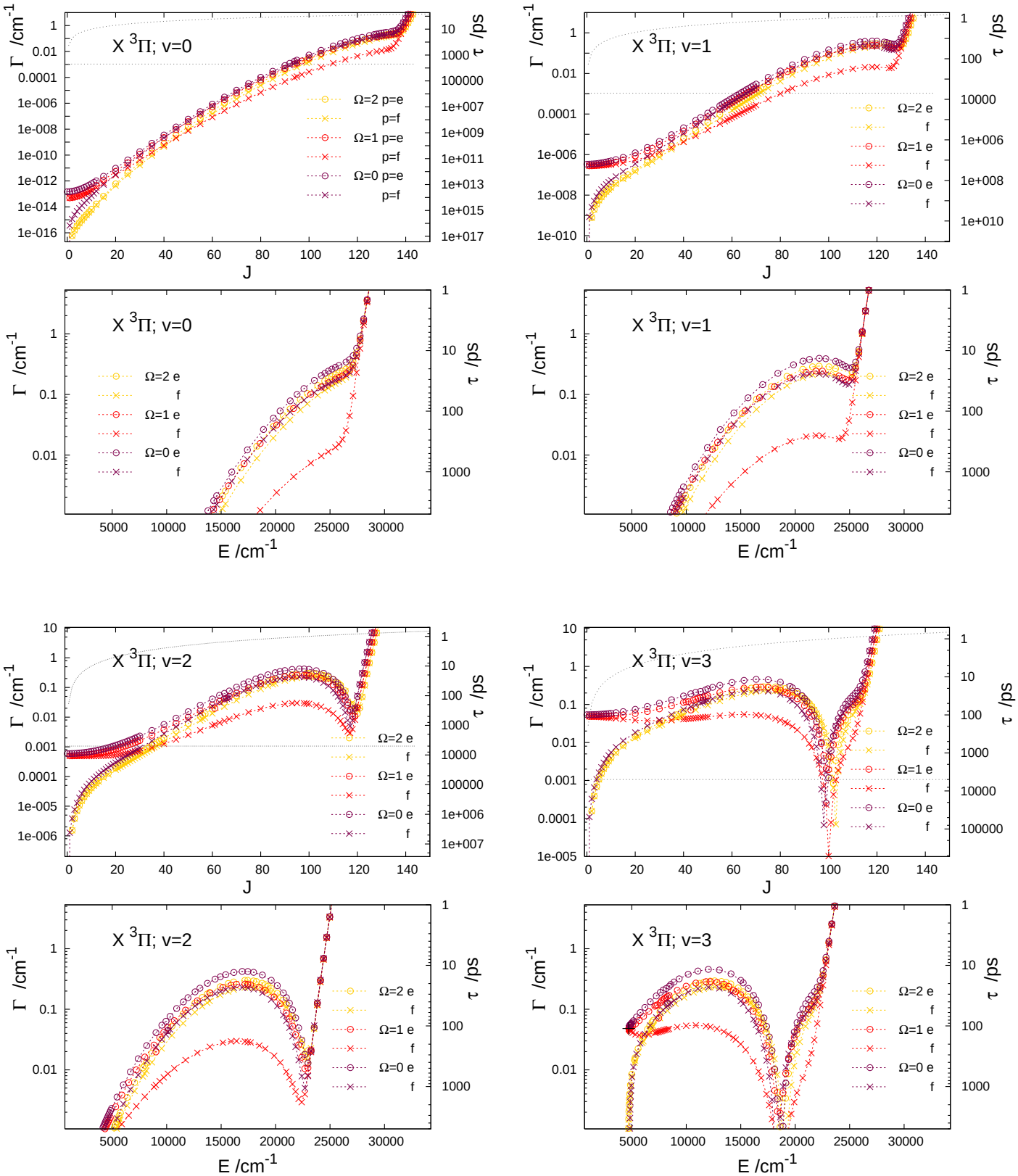

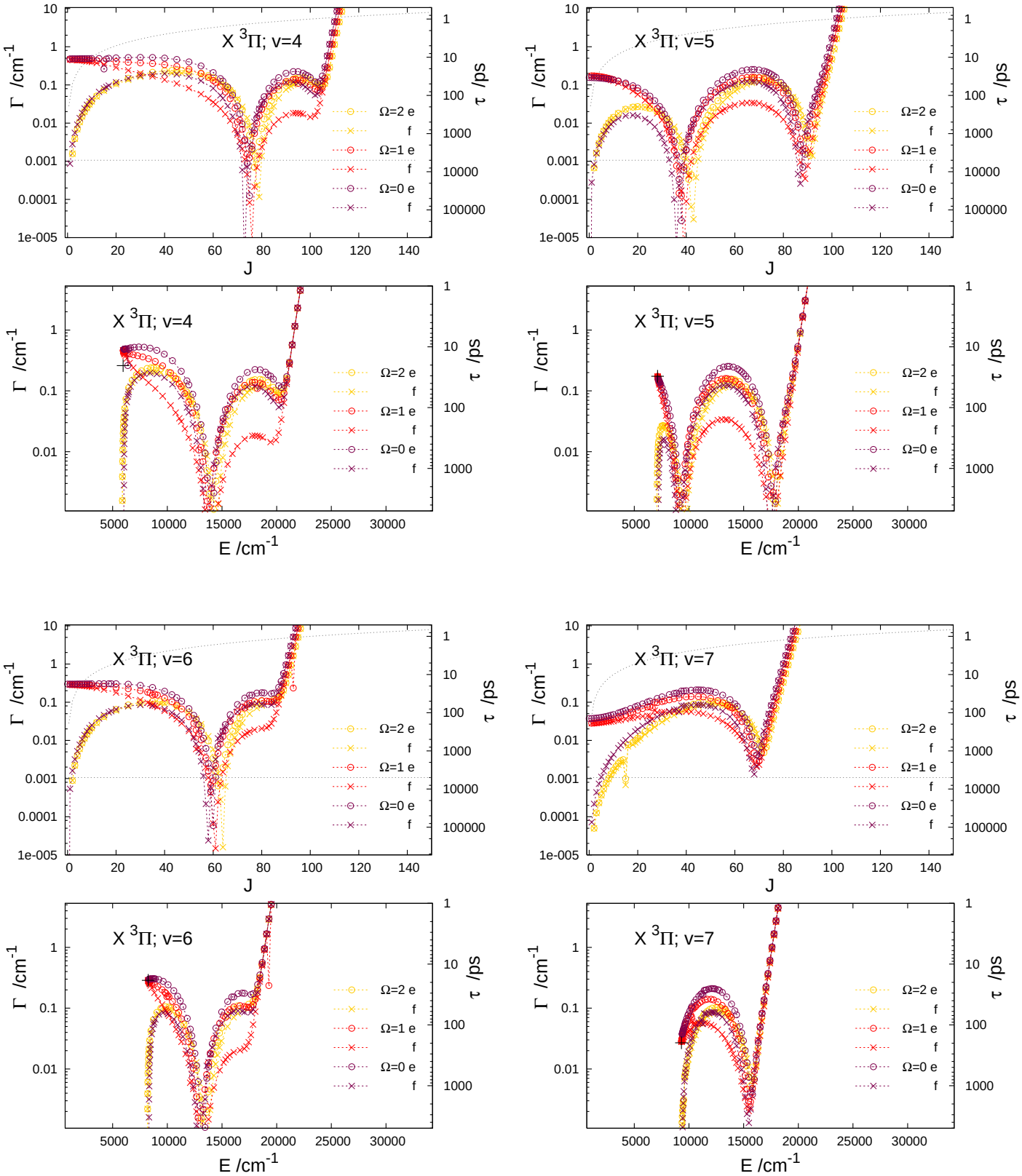
X 3Π; v=4
X 3Π; v=5
X 3Π; v=6
X 3Π; v=7
Γ /cm-1
τ /ps
J
E /cm-1
Ω=2 e
f
Ω=1 e
f
Ω=0 e
f

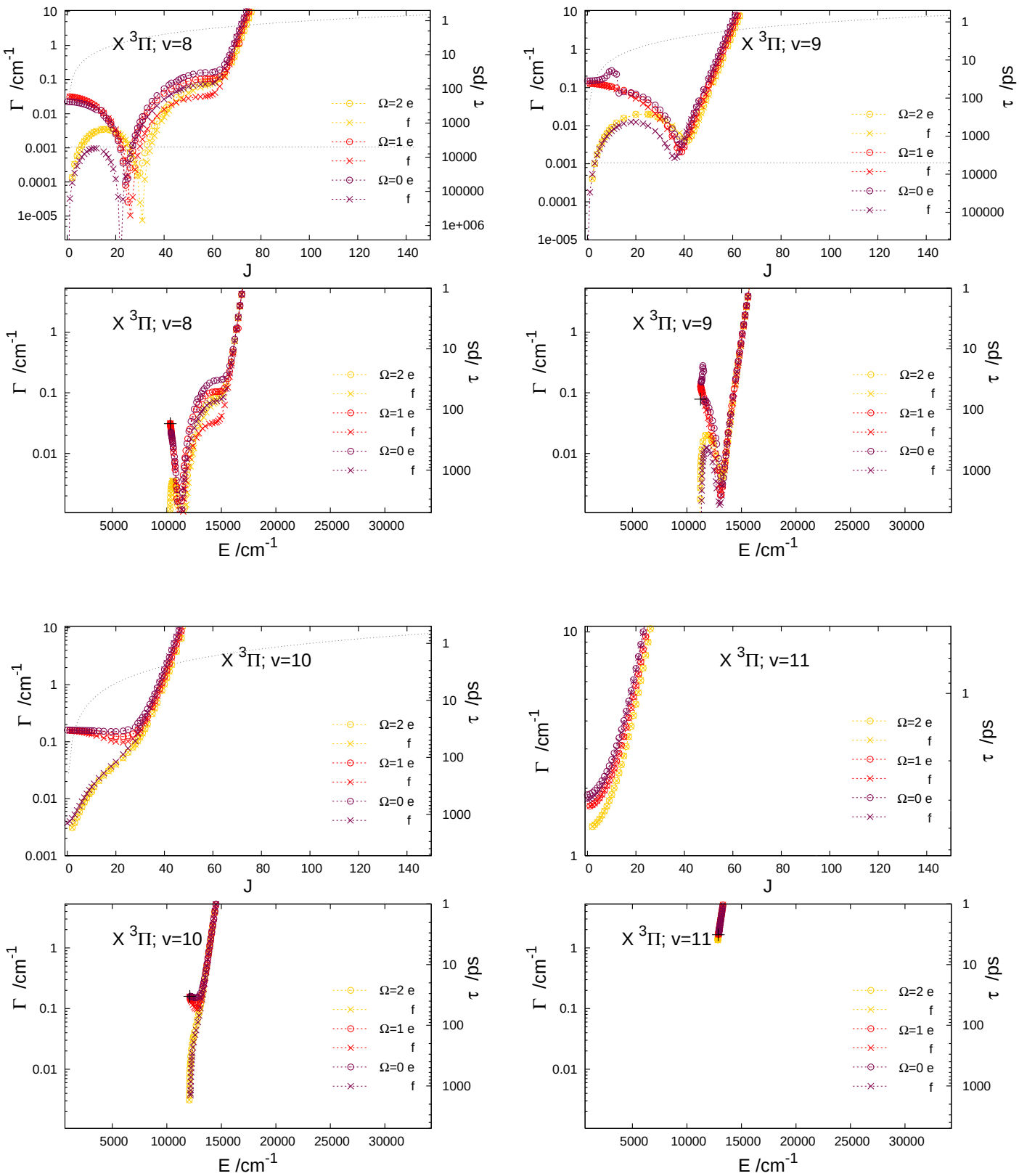

The dotted lines in the upper panel of each $X\,v$ state here, and of other $s\,v$ states in Figs. A3b-A3d and A4a-b, show the lifetime interval of $100/J$ ps — 5 ns; levels from this interval are included into the distributions DOS(E), DOL(E), and the related KER spectra presented in Figs. 5-8 of the paper and in Figs. A5-A8 of this material. In the lower panels, the widths as functions of E_J are shown only in the range of interest.

Fig. A3b. $CO^{2+}(a\,^1\Sigma^+)$

Widths of vJ levels

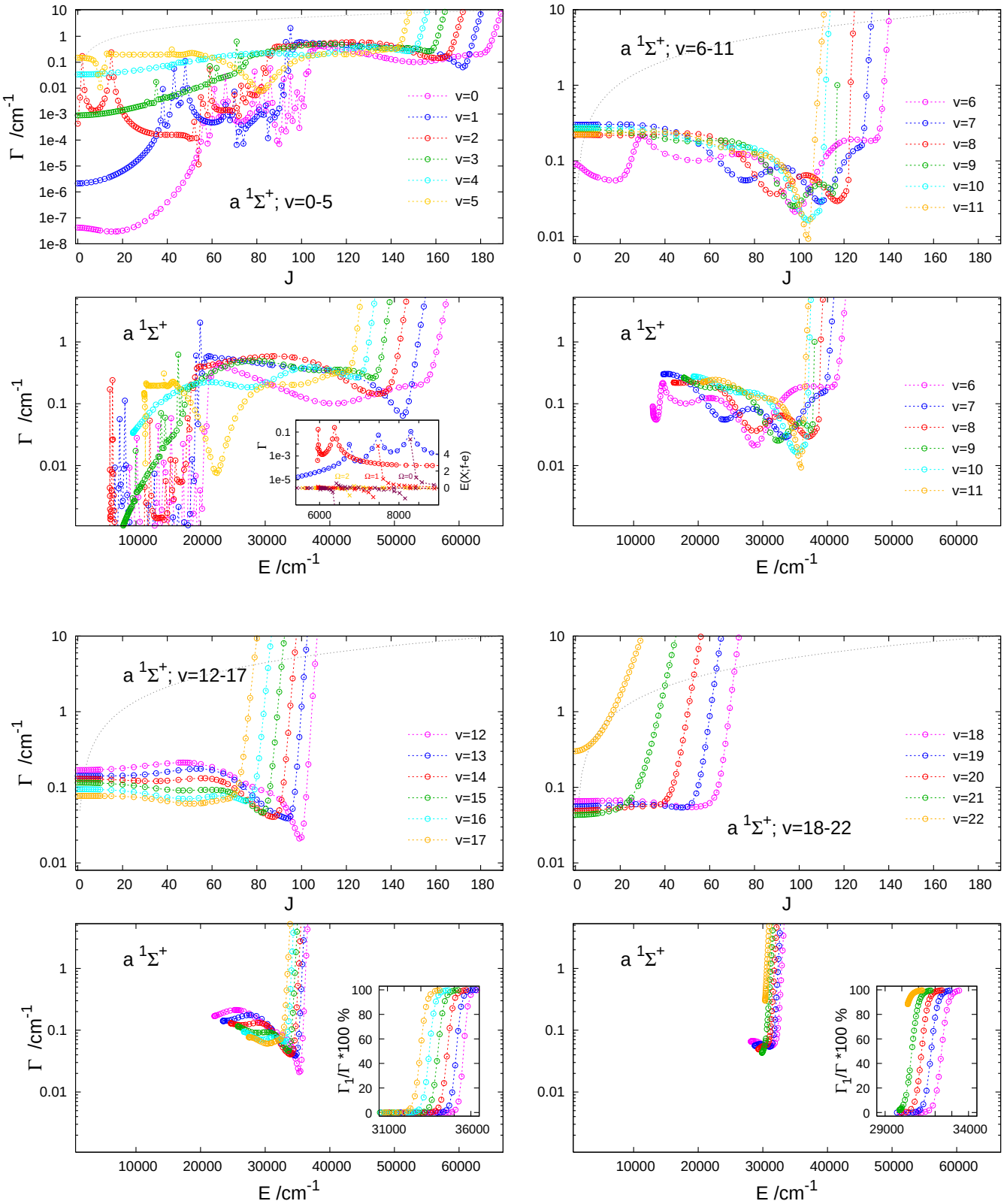

The peaks in the functions $\Gamma(J)$ or $\Gamma(E_J)$ of the states $a\,^1\Sigma^+$ v=0−3 are due to accidental near-degeneracies with some E_J levels of the states $X\,^3\Pi_{\Omega=0-2}$ v=2−8. Since only e-parity states are involved in the $X-a$ interaction, see Fig. A1, the responsible cases of the accidental degeneracy/perturbation can be found easily by inspecting the $f-e$ splitting of the X-state energy levels listed in Table BI. An example is shown here in the inset of the left second-row panel. The three peak in the function $\Gamma(a\,v{=}1;\,E_J)$, at J=38, 43, and 48, occur at the "jumps"/poles in the functions $E_J(X\,\Omega\,v{=}3;\,f-e)$ for Ω=2, 1, and 0, respectively.

Fig. A3c. $\mathbf{CO^{2+}}(b\,^1\Pi)$

Widths of vJp levels

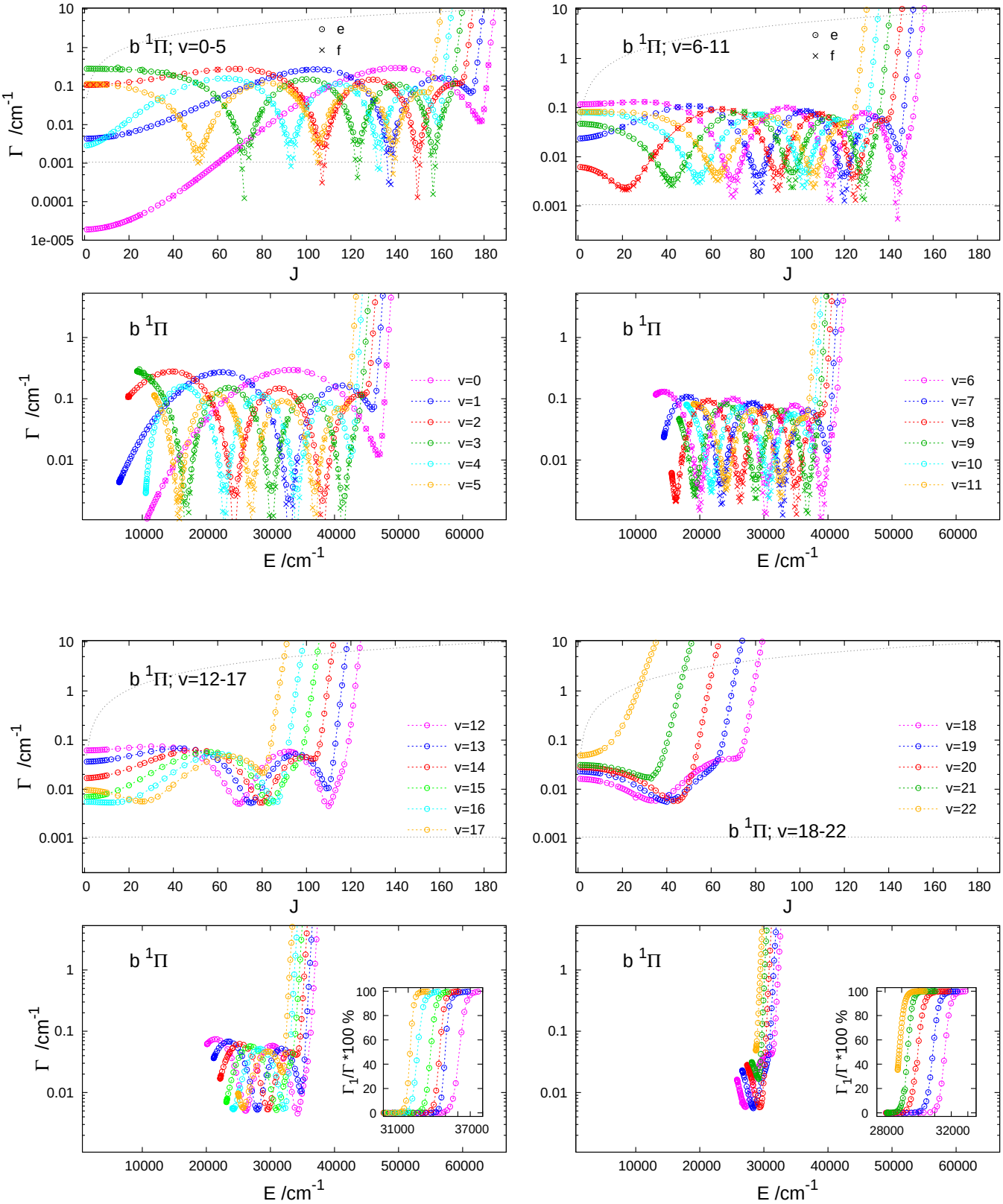

In the insets of the two lowest panels, here and in Fig. A3b, shown are exemplarily the probabilities of populating the first excited C^++O^+ channel. The rapid increase with the rotational energy of these probabilities from 0 to nearly 1 accompanies the rapid growth of the width functions $\Gamma(E_J)$ in their large J parts. Both effects are manifestations of tunneling taking over the leading role in the dissociation the ion. Tunneling is the only mechanism by which the first excited fragmentation channel can be reached in the dissociation from the states $a\,vJp$, $b\,vJp$ and $c\,vJp$ (the latter are demonstrated in Fig. A4a).

Fig. A3d. $CO^{2+}(A\,^3\Sigma^+_\Omega)$

Widths of vF_iN levels

$$F_1\,N \;:=\; \Omega{=}1, J{=}N{+}1, p{=}f$$
$$F_2\,N \;:=\; \Omega{=}1, J{=}N \quad\;\; , p{=}e$$
$$F_3\,N \;:=\; \Omega{=}0, J{=}N{-}1, p{=}f$$

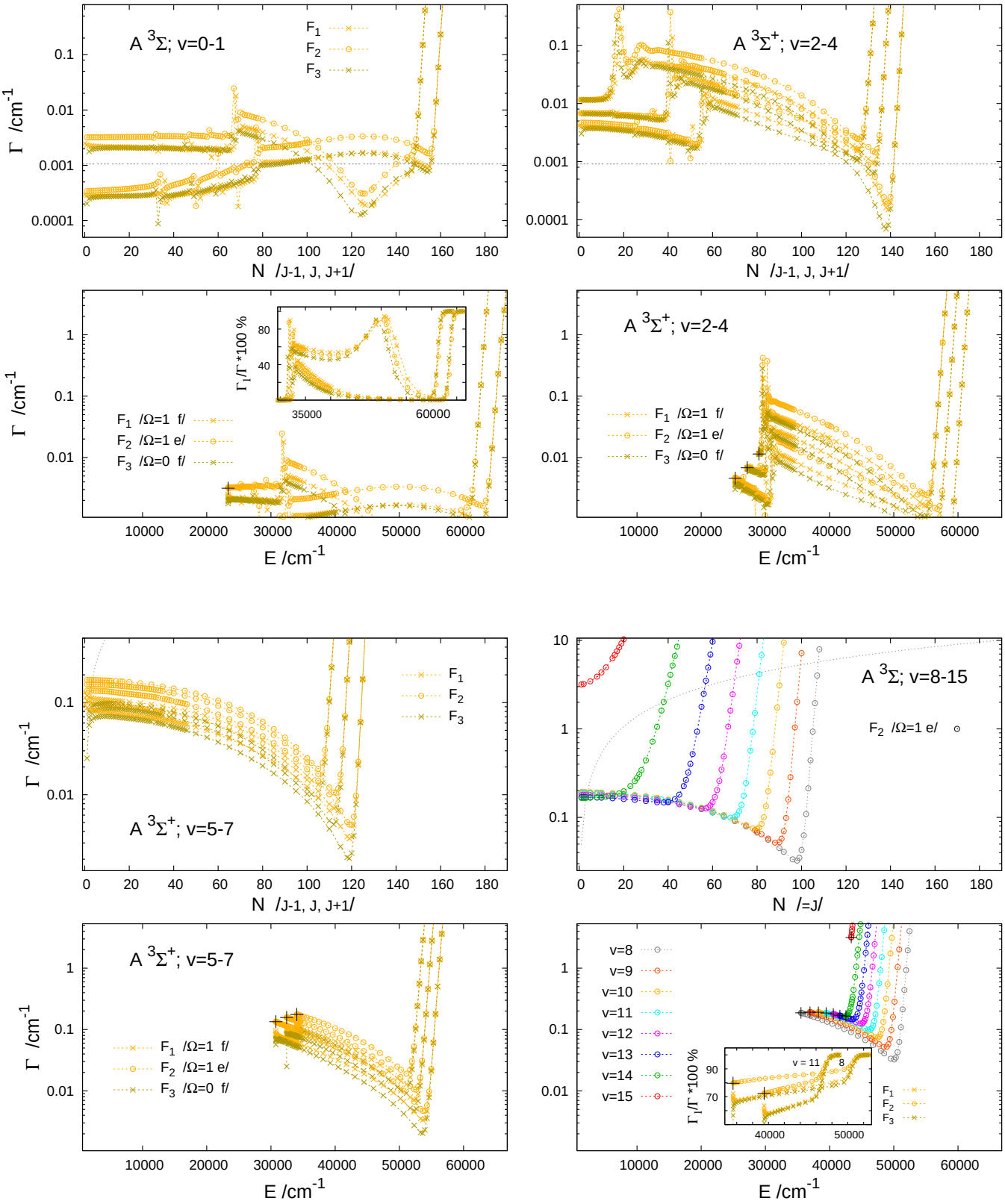

Fig. A3e. Widths functions $\Gamma(E_{Jp})$ in selected vibronic states

Contributions of curve crossings♯ and tunneling♮

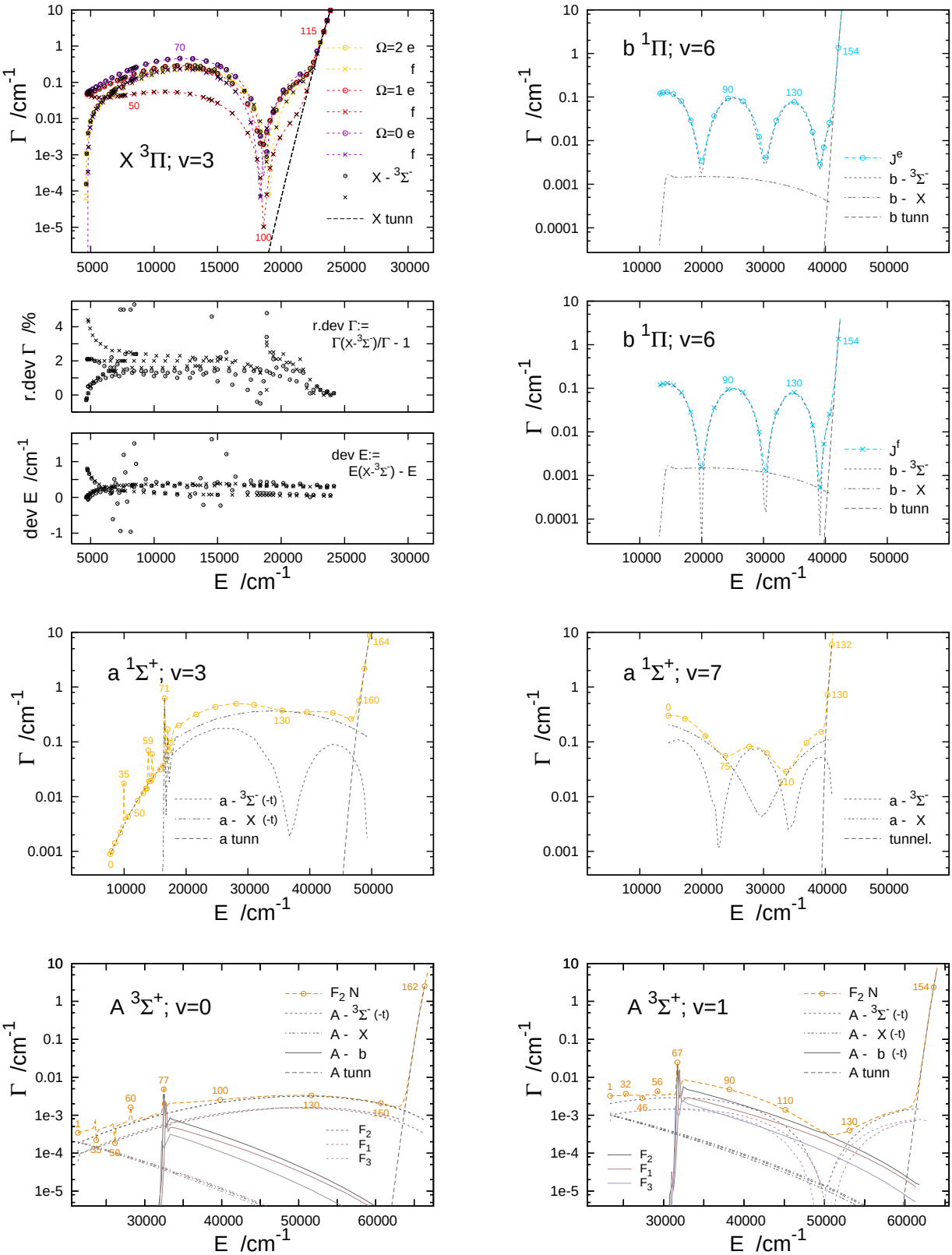

♯ The contribution of a given crossing $s-\widetilde{s}$ is evaluated in calculations using only sub-matrices of the Hamiltonian matrices $\mathbf{H}^{Jp}$ for p=e, f which include the blocks of the states s and $\widetilde{s}$, the rotational couplings within the two blocks, and the SO couplings between them. The partial widths, due to the individual crossings, which result from these calculations, sum up to the total 'exact' predissocition widths with deviations usually smaller than 5%, similar to the deviations shown here for levels in the state X v=3.

♮ Obtained by using one diagonal element of $\mathbf{H}^{Jp}$ from the block s.

Fig. A4a. $CO^{2+}(c\,^1\Delta)$

Energies and widths of vJe/f levels*

Selected effective potentials $V^J_{s\Omega}(r)$:=$V^{Jp}_{s\Omega,s\Omega}(r)$ used in the calculations on the levels, see Fig. A1. The outer parts of the barriers in the potentials $V^J_c(r)$, at r>4.6a_0, are only a crude extrapolation of the data available on the electronic potential $V_c(r)$ from Ref. 3. Details are given in Table BV.

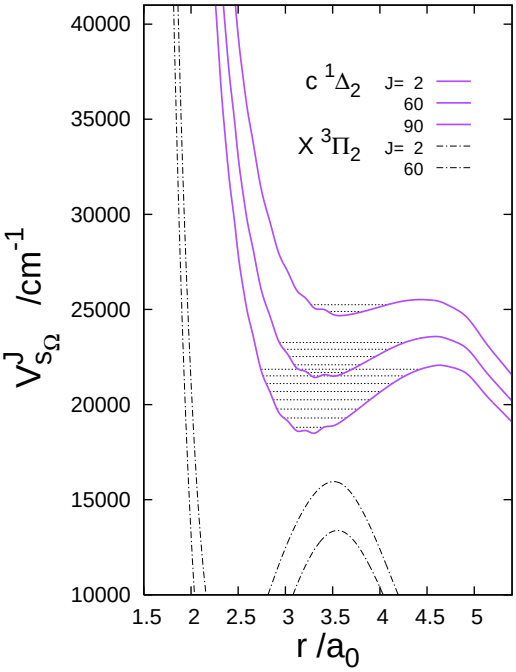

* Levels of both parities have in the model practically the same energies and the same widths. See Table BV.

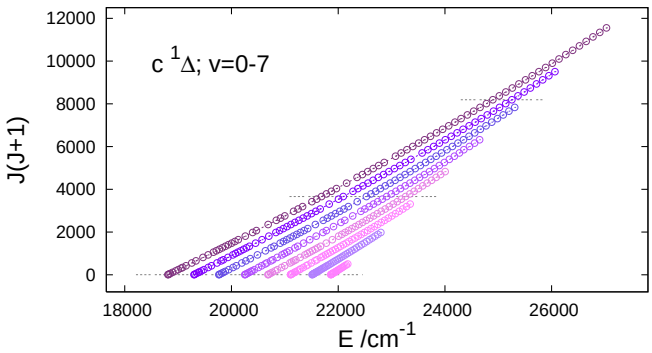

Levels lying on the horizontal dotted lines are shown within the potentials $V^J_c(r)$ in the upper panel.

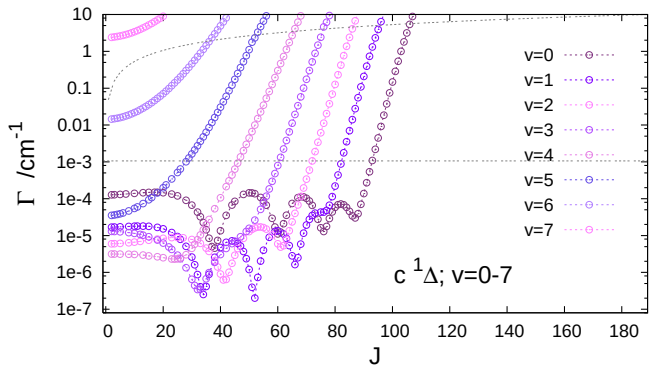

About 1100 levels of both parities were found whose widths are below the assumed upper limit of 10.6 cm^{-1} (Not all of them are represented by a circle in the left upper and middle panels.) About 1/4 of these levels have widths in the range between the dotted lines and can therefore contribute to the KER spectra determined in this work.

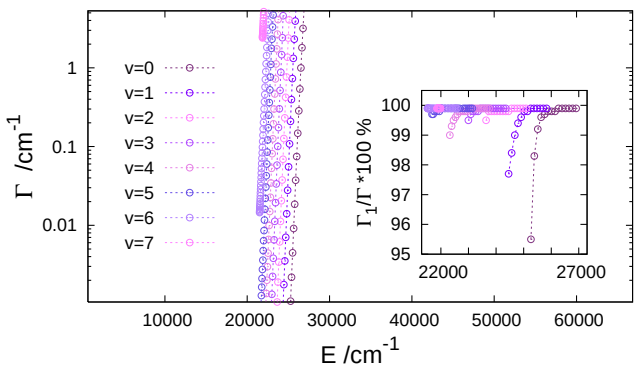

As shown in the inset, nearly all of the contributing levels decay almost entirely to the first excited fragmentation channel, i.e. by tunneling.

Fig. A4b. $CO^{2+}(d\,^1\Sigma^+)$

vJ levels

of widths in the range $\sim 5\times10^{-5} - \sim 25$ cm^{-1}

due to tunneling only ....

Effective potentials $V_d^J(r)$, for several values of J, used in the calculations on the levels. The potential $V_d^{J=0}$ comes from interpolation between the points generated ab initio in Ref. 3 and, for $r>4.4\,a_0$, from an extrapolation of these data. Accuracy of the extrapolation is rather uncertain. [Two ab initio values, at r=2.4 and 2.45 A, were severely altered in order to produce the reasonably smooth curve]. The asymptote of the potential lies[3] 1.866 eV above the common asymptote of the states a, b, c and A.

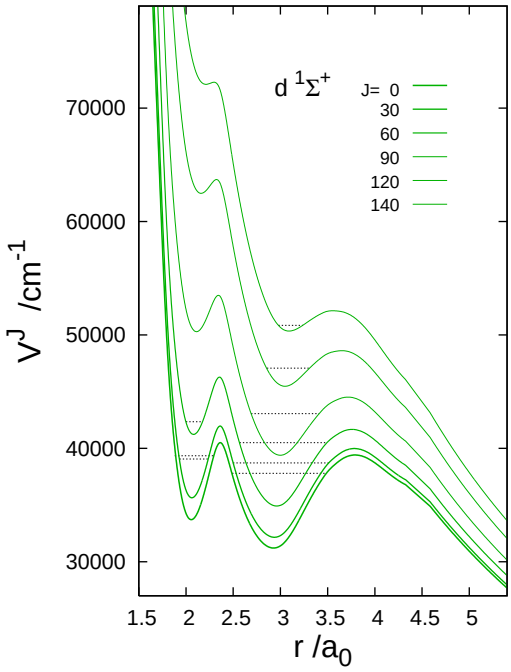

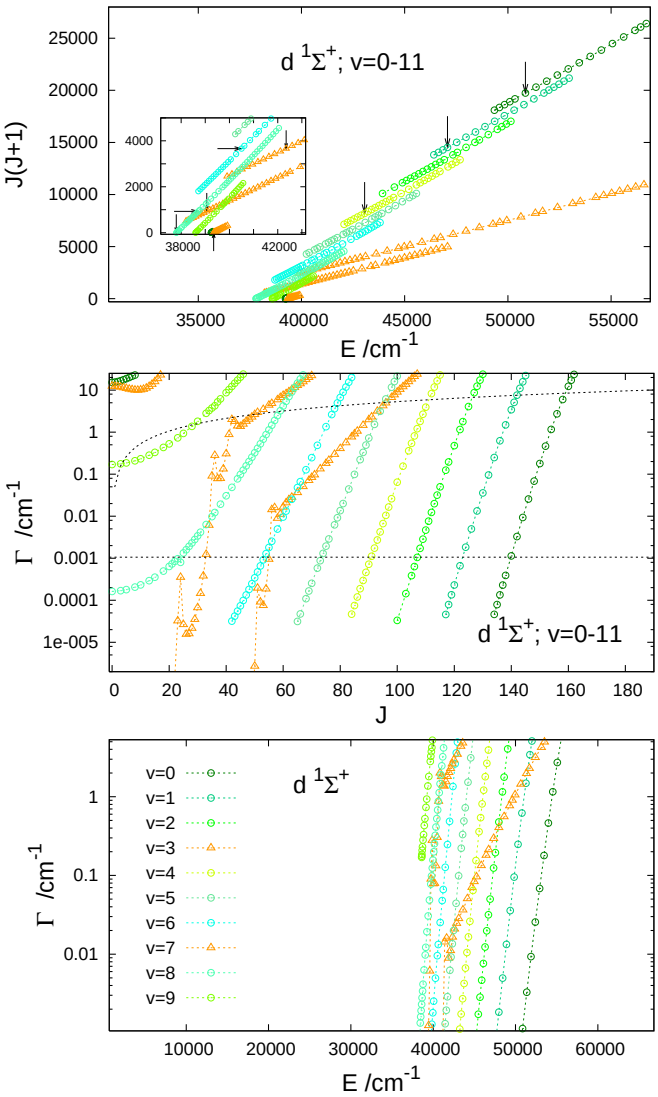

The arrows indicate the levels whose location within the respective potential V^J is shown in the upper panel. Even the lowest of these levels (v=8 J=0) should not be affected by the extrapolated part of the potential V^0. The number v is assigned here according to ordering of J=0 levels, $E_v<E_{v+1}$ for $v=0,\ldots,11$. Levels supported by the inner wells of the potentials V^J are shown by the orange triangles.

As obvious, energies and widths of the inner-well levels behave differently upon the increase of the number J than the characteristics of the levels supported by the outer well. The energies grow faster because of approximately two times larger rotational constant[3]. The widths grow with different rates depending on whether both barriers or only the inner one is penetrated. The spikes in the orange $\Gamma(J)$ and $\Gamma(E_J)$ curves are due to accidental near-degeneracy with an outer-well level, see Table BVI.

Altogether, 1002 levels exist in the used potentials V_d^J whose widths are below 10.6 cm^{-1}. Only 243 of them are relevant to the calculated KER spectra (lie in the width range between the dotted lines).

... possible effects of predissociation

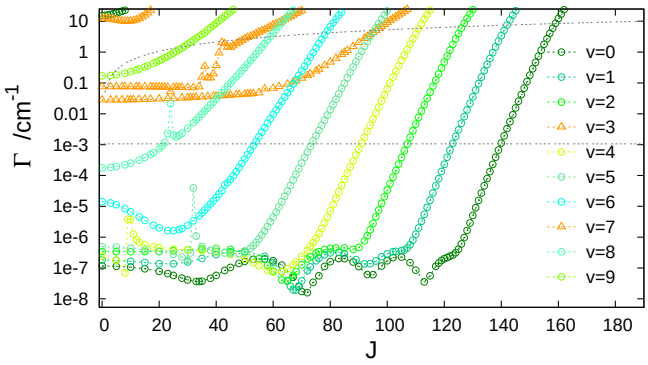

Widths due to tunneling and predissociation of $v\,J$ levels in both wells of the d state potential. Due to the fast predissociation from the inner well, the number of levels characterized by Γ in the range between the dotted lines increases (to 348, i.e. by 8.5%). Since the lowest C^++O^+ channel is reached in the predissociation, the v=3 J<55 and v=7 J<∼30 levels would increase slightly the distributions KERS(e) and KERL(e) shown in Figs. 6b and 8b of the paper at e=∼9.5−10.3 eV. A competition between predissociation and tunneling in the decay of the inner-well levels with higher J values would result in a slight relocation of the d state contributions to higher e region. Unfortunately, the troublesome feature around e=5 eV (least similar in the relative size to the feature in the experimental spectrum[2]) would become slightly reduced.

Widths obtained in calculations with the Hamiltonian matrix $\ddot{\mathbf{H}}^{Je}$, see Fig. A1.

Below: Examples of involved effective potentials $V^J_{s_{\Omega=0}}$ (for J=1 and J=30) and the important outer-type crossings with the inner wells of the potentials V^J_d. Shown are also the two lowest levels supported by these wells whose widths become enlarged by orders of magnitude due to the $d-{}^3\Sigma^-$ crossings.

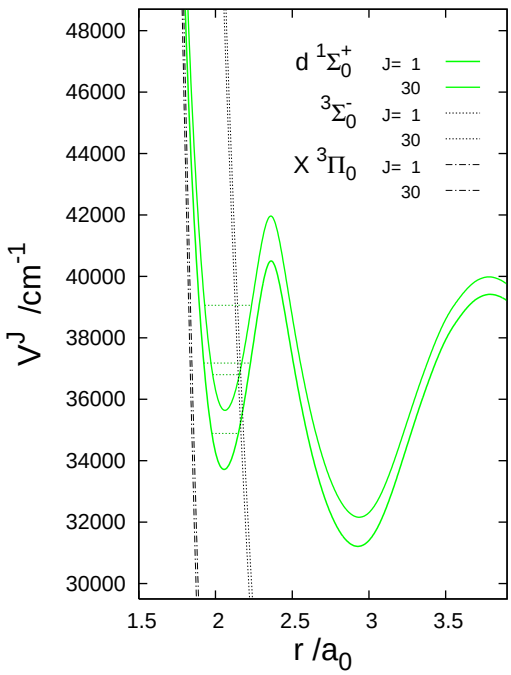

$\mathbf{CO}^{2+}(X\,^3\Pi, a\,^1\Sigma^+, b\,^1\Pi, A\,^3\Sigma^+)$

Fig. A5. Densities of rovibronic energy levels $^{2S+1}\Lambda_\Omega\, vJp$ /DOL/ in the range up to ∼13.5 eV above the lowest atomic limit for three ranges of level widths

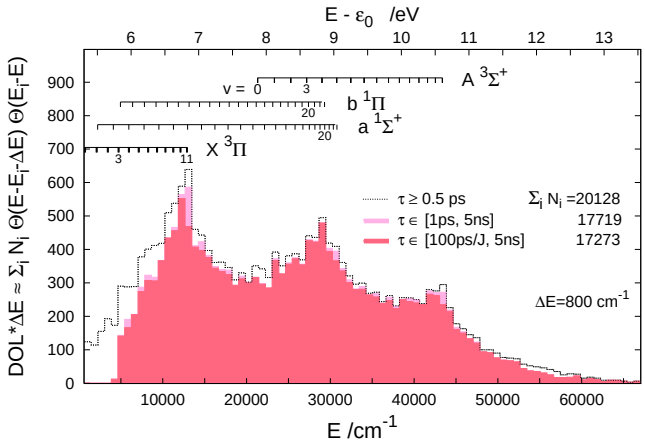

. . . resolutions into contributions of the four included electronic and 74 vibronic states

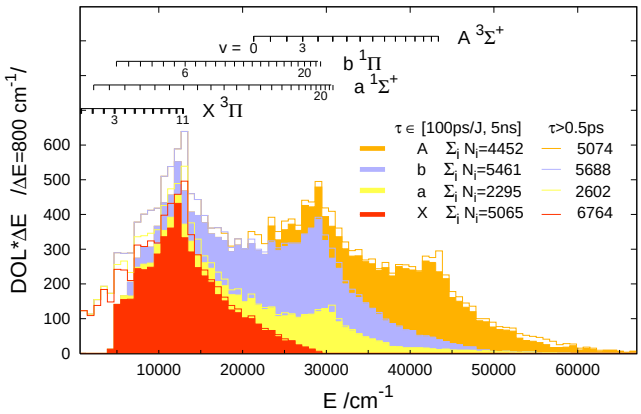

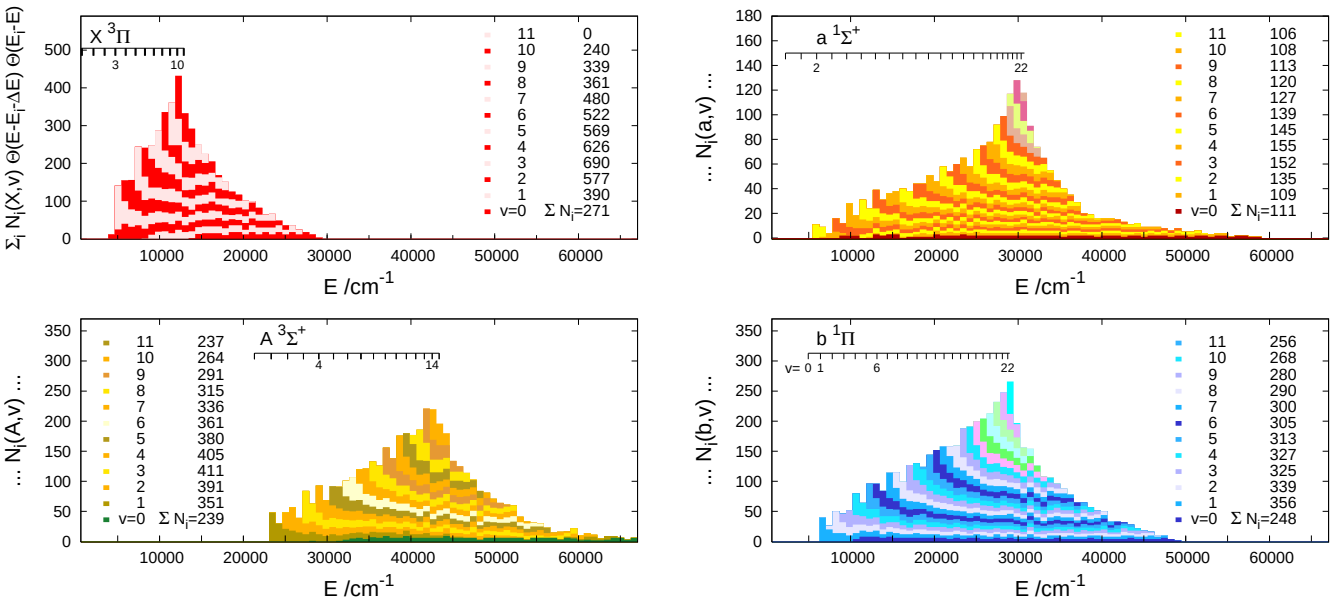

Fig. A6. Kinetic energy release spectrum from decay of the rovibronic levels / KERL(e) /

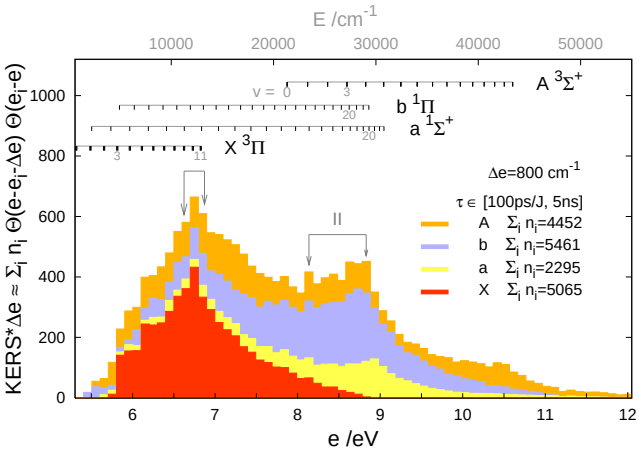

. . . contributions of Jp levels from different vibronic states $s\,v$

for s=$X\,^3\Pi$, $a\,^1\Sigma^+$, $b^1\Pi$, $A\,^3\Sigma^+$

/summation over Ω components of the triplet states included/

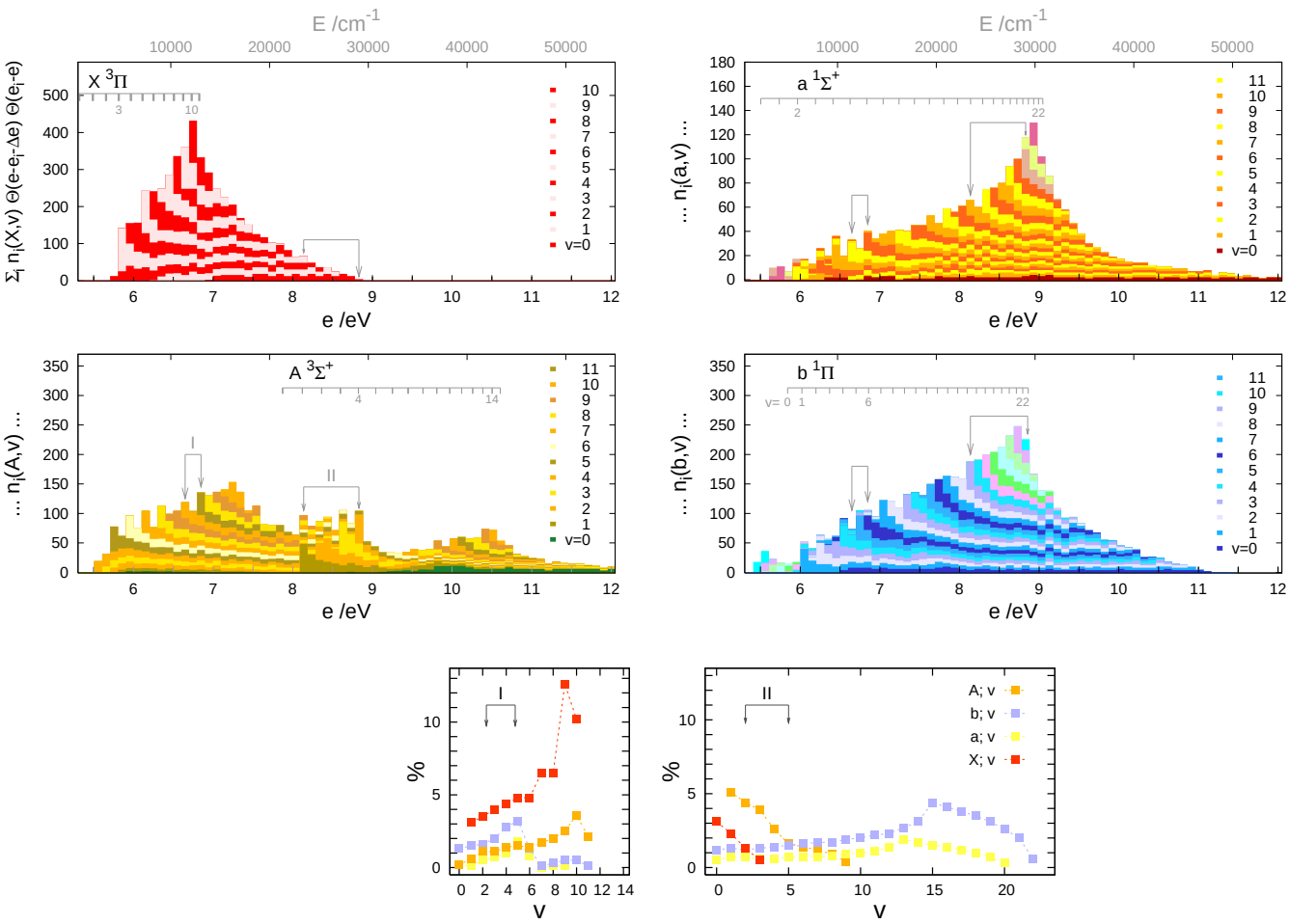

... percentage contributions of the particular vibronic states in the regions of the main and secondary maxima of the KERL(e)

Fig. A7. Densities of rovibronic states $^{2S+1}\Lambda_\Omega\, vJMp$ /DOS/

for two ranges of their lifetimes

— resolutions into contributions of the ΩJMp sub-states of the four electronic s=$X^3\Pi, a^1\Sigma^+, b^1\Pi, A^3\Sigma^+$

and 74 vibronic sv states

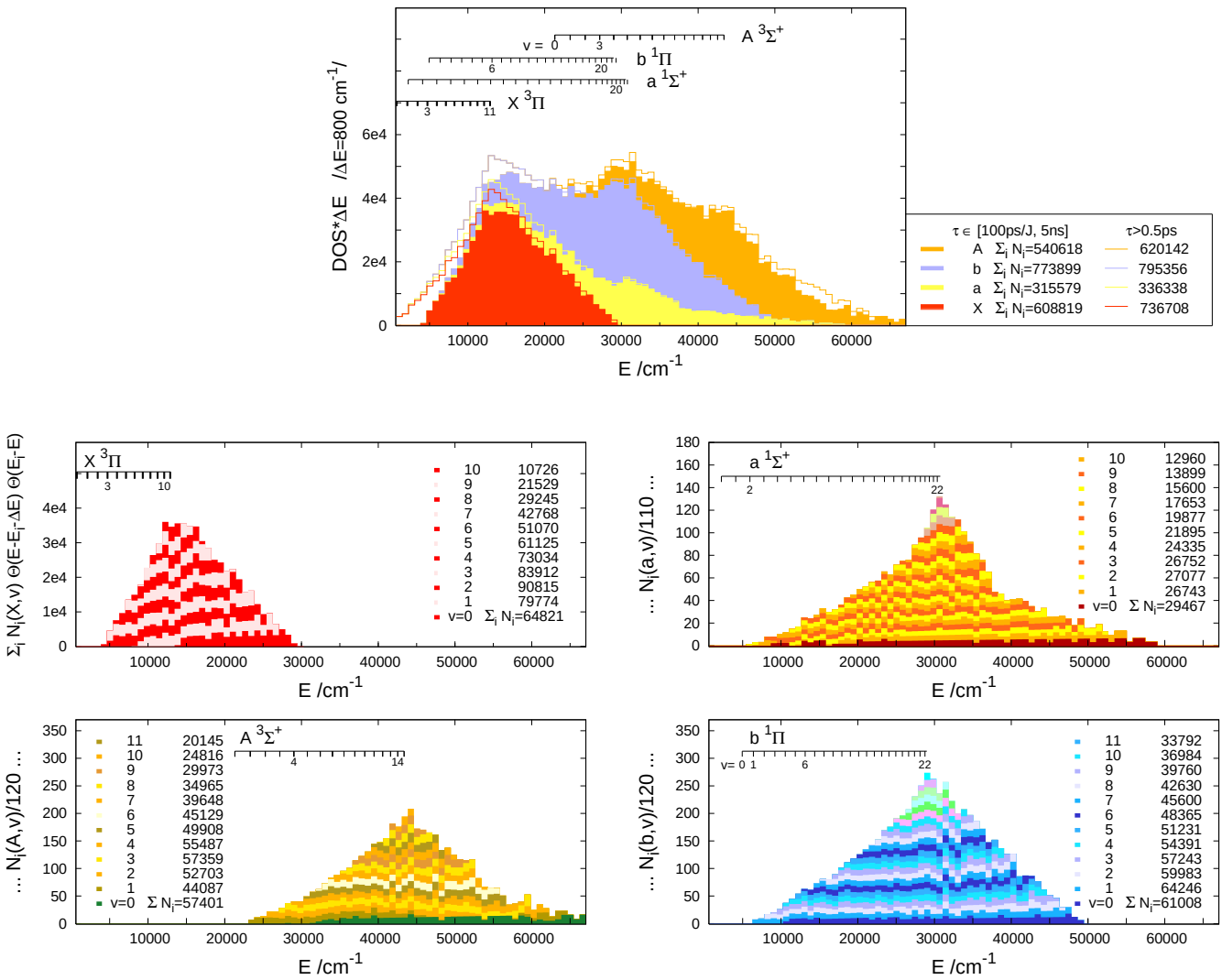

Fig. A8. Kinetic energy release spectrum from decay of the rovibronic states

/ KERS(e) /

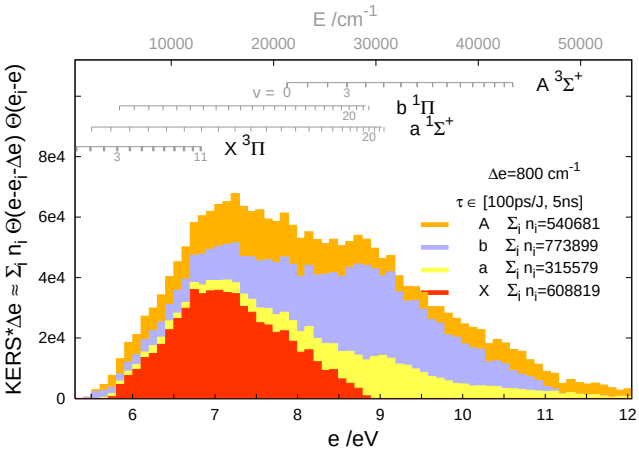

. . . contributions of the different vibronic states

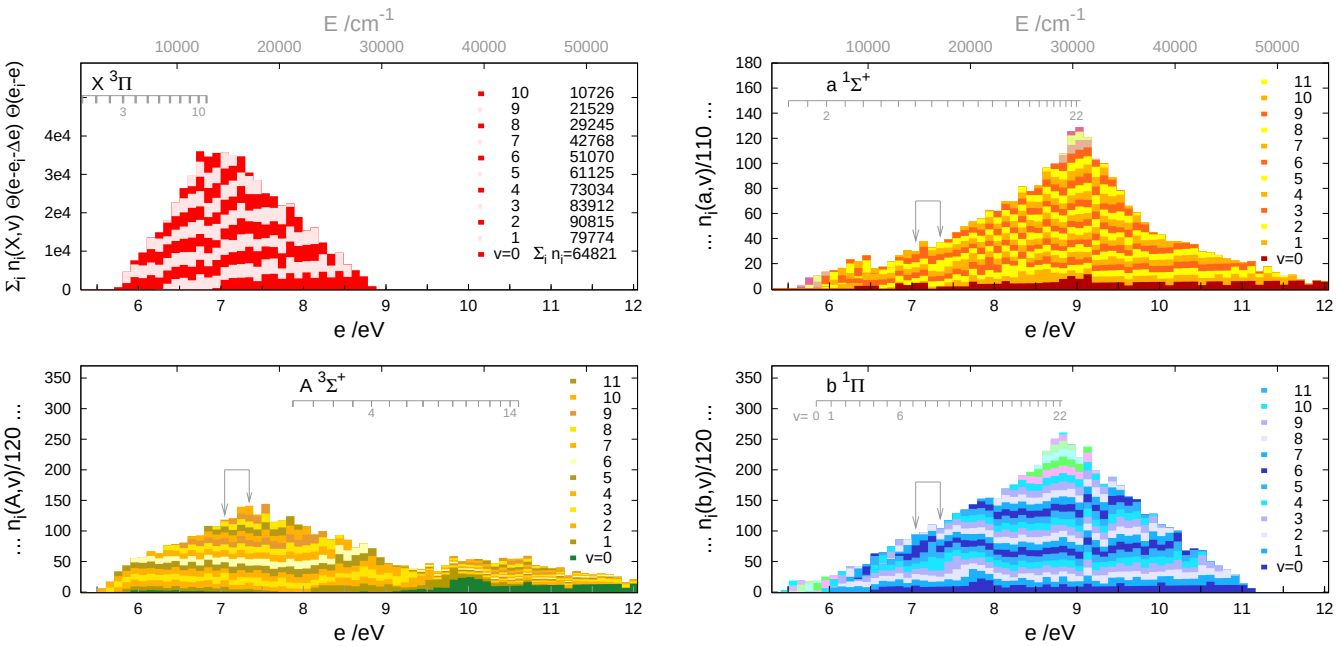

[1] Herendra Kumar, Pragya Bhatt, C. P. Safvan, and Jyoti Rajput, J. Chem. Phys. **148**, 064302 (2018); J. Phys.: Conf. Ser. **875**, 102006 (2017).
[2] Joyti Rayput, T.Severt, Ben Berry, Bethany Jochim, Peyman Feizollah, Balram Kaderiya, M.Zohrabi, U. Ablikim, Farzaneh Ziaee, Kanaka Raju P., D. Rolles, A. Rudenko, K. D. Carnes, B. D. Esry, and I. Ben-Itzhak, Phys. Rev. Lett. **120**, 103001 (2018).
[3] J. H. D. Eland, M. Hochlaf, G. C. King, P. S. Kreynin, R. J. Le Roy, I. R. McNab, and J. M. Robbe, J. Phys. **B 37**, 3197 (2004).
[4] T. Šedivcová, P. R. Ždánská, V. Špirko, and J. Fišer, J. Chem. Phys. **124**, 214303 (2006).
[5] F. Mrugała and D. Secrest, J. Chem. Phys. **79**, 5960 (1983); F. Mrugała, Int. Rev. Phys. Chem. **12**, 1 (1993).
[6] B. Barmore, A. T. Kruppa, W. Nazarewicz, and T. Vertse, Phys. Rev. **C62**, 054315 (2000).
[7] F. Mrugała, J. Comput. Phys. **58**, 113 (1985).
[8] F. Mrugała, J. Chem. Phys. **93**, 1257 (1990).
[9] B. R. Johnson, J. Comput. Phys. **13**, 445 (1973).
[10] F. Mrugała, J. Chem. Phys. **129**, 064314 (2008).